Synthetic torpor in the rat recapitulates key features of natural torpor and protects the heart from ischaemia-reperfusion injury

Megan Elley[1], Ludovico Taddei[2], Muz Ali Khan[1], Una R Wilcox[1,3], Timna Hitrec[2], Anthony Pickering[1], Michael Ambler[1]

Abstract:
During hibernation, animals enter torpor, a reversible physiological state typically characterised by reductions in core temperature, heart rate and oxygen consumption. Species that enter this hypothermic and hypometabolic state are highly tolerant of ischaemia-reperfusion injury. Consequently, there is a growing interest in utilizing aspects of torpor for clinical applications, such as protection from ischaemia-reperfusion injury during stroke or myocardial infarction. It is currently unknown, however, if a torpor-like state is protective in animals that do not naturally enter torpor. Using viral-vector mediated chemogenetics in the medial preoptic area of the hypothalamus, we induced synthetic torpor in the rat, a species that does not naturally enter torpor. We demonstrate this state is cardioprotective in an ex-vivo ischaemia-reperfusion injury model. Synthetic torpor induced cardioprotection of the normothermic, isolated heart is not dependent on hypothermia during synthetic torpor. These findings provide important insights into synthetic torpor states in novel species, and demonstrate feasibility for future clinical translation in humans.

Introduction:
Cardiovascular disease, including stroke and myocardial infarction, is the leading cause of death and disability globally[1,2]. Most current treatment strategies focus on re-establishing tissue perfusion, but there is interest in developing alternative strategies to improve tolerance to the ischaemia or to reduce the impact of the reperfusion injury[3]. The idea that therapeutic hypothermia might reduce cell death during ischaemia-reperfusion has remained popular for many years, fuelled by encouraging animal studies[4–8]. However, despite early positive trials[9], more recent clinical data do not support the hypothesis that induced-hypothermia improves outcomes following cardiac arrrest[10]. Failure to translate benefits from animal studies to adult clinical conditions may be due to side-effects arising from the counter-regulatory reflexes triggered by physical cooling. These reflexes lead to: haemodynamic instability; shivering with increased oxygen consumption; cardiac arrhythmias; and electrolyte and glucose disturbances[11,12]. Hence, interest is growing in centrally driven hypometabolic, hypothermic states that might avoid these counter-regulatory responses. With this in mind, researchers have turned to hibernating animals as a model for a centrally driven protective hypometabolic state[8,13–15].

During hibernation, animals enter torpor, which is a remarkable physiological adaptation typically characterised by rapid and profound reductions in core temperature, heart rate, and oxygen consumption[16]. Torpor can be prolonged, in seasonal hibernators, or brief in daily heterotherms such as the mouse. It serves as a protective adaptive response to relative energy deficit achieved via a controlled reduction in metabolic demand in response to reduced availability of substrate. During torpor, body temperature can be lowered to a few degrees above ambient temperature[17,18]. Metabolic activity may fall to 5% of the euthermic rate, with active and profound decreases in cardiac output, and minute ventilation, all of which rapidly return to 'normal' values on arousal without harm to the individual[17,18]. Seasonal hibernators spend prolonged periods of time torpid and are highly tolerant of ischaemia-reperfusion injury[13,19,20]. Therefore, developing biomimetic torpor-like states for clinical applications might provide a wide range of benefits including protection from ischaemia-reperfusion injury[15].

A fundamental hypothesis underlying interest in such translational torpor research is that conserved mechanisms exist in species that do not naturally enter torpor (potentially including humans), aspects

of which might be harnessed to improve clinical outcomes. There are several reasons to suppose this to be the case. Firstly, torpor is extremely widespread, seen in all classes of vertebrate life, including primates[18,21]. Secondly, a unique torpor gene (or complement of genes) has so far not been described. Rather, those mammals that enter torpor do so through activation of ubiquitous genes[22–24]. Thirdly, body temperature is not fixed even in 'strict' homeotherms: non-rapid-eye-movement sleep (NREM) is a controlled state of reduced body temperature and inactivity, features it shares with torpor[25,26].

Attempts to induce a "synthetic" torpor-like state in a species for which it is not a natural behaviour have focused on the rat, and include inhibition of the rostral ventromedial medulla[27]; peripheral infusion of drugs, such as adenosine and neurotensin analogues[28,29]; and targeted activation of neurons in the preoptic area of the hypothalamus[30]. Of these approaches, the latter is arguably the closest to mimicking natural torpor, since it engages neurons in part of the hypothalamus that drives entry into natural torpor in mice[30–32].

We sought to characterise the state of synthetic torpor induced in the rat by targeted activation of neurons in the hypothalamic medial preoptic area (MPA), and to test the hypothesis that induction of synthetic torpor protects the heart from ischaemia-reperfusion injury.

Results:

Induction of biomimetic synthetic torpor in the rat

We used viral vector-mediated chemogenetics to selectively activate neurons in the MPA (figure 1A). The vector (AAV-CaMKIIa-hM3D(Gq)-mCherry) was injected bilaterally into the rat MPA, resulting in local expression of the modified receptor hM3Dq (a Gq-coupled Designer Receptor Exclusively Activated by Designer Drug, DREADD[33,34]) under the control of the CaMKIIα promoter[35,36] (MPA^{Gq}). Control animals underwent identical procedures but received injection of AAV-CaMKIIa-EGFP into the MPA which results only in the expression of a green fluorescent protein (MPA^{EGFP}).

Subsequent MPA neuronal activation using intraperitoneal CNO (2 mg/kg) induced a rapid and reversible decrease in core temperature (mean temperature post-CNO in MPA^{Gq} rats 31.64 ± 1.02°C vs MPA^{EGFP} rats 37.05 ± 0.43°C, p <0.0001, see Figure 1B). This was accompanied by a 24% lower heart rate (mean heart rate post-CNO in MPA^{Gq} rats 260 ± 44 bpm vs MPA^{EGFP} 342 ± 32 bpm, p <0.005, figure 1C). This was associated with a 43% reduction in oxygen consumption (mean oxygen consumption prior to CNO 2.14±0.26ml/g/hr vs 1.23±0.41ml/kg/hr post CNO, p =0.026, figure 1D). Hence, chemoactivation of neurons in the rat MPA produces a synthetic torpor state that recapitulates three key features of natural torpor: hypothermia, bradycardia, and reduced oxygen consumption.

Characterising the neurons in the rat MPA responsible for inducing synthetic torpor

To establish whether the neurons involved in inducing this synthetic torpor state are excitatory or inhibitory, we used in situ hybridization (ISH) to examine colocalization of vector-mediated *mCherry* expression (Figure 2A) with genes that encode vesicular glutamate transporter 2 (*Vglut2*, gene ID *Sl17a6*) and vesicular GABA transporter (*Vgat*, gene ID *Slc32a1*) (Figure 2B). We found a large proportion of transduced neurons expressed *Vglut2* (72%, Figure 2C). We also detected a population of neurons, termed "hybrid" neurons, (that co-express both excitatory and inhibitory markers), that were positive for *mCherry, Vglut2* and *Vgat* (35%) (Figure 2C). A small proportion of *mCherry* neurons were inhibitory (14%), expressing *mCherry* and *Vgat* and some *mCherry* neurons expressed neither *Vglut2* nor *Vgat* (15%) (Figure 2C).

Previous studies have identified a population of neurons within the preoptic area of the hypothalamus of mice, which can integrate stimuli to regulate thermogenesis and metabolism and induce a hibernation-like state upon activation[37]. These stimuli include temperature changes both locally within the hypothalamus and from peripheral signals in the skin, inflammatory prostaglandin signalling,

leptin, oestrogen, and violet light. These neurons have been termed QPLOT neurons, due to their co-expression of neuropeptide pyroglutamylated RFamide peptide (Qrfp), Prostaglandin EP3 receptor (encoded by *Ptger3*), Leptin receptor (encoded by *Lepr*), violet light-sensitive opsin, Neuropsin (encoded by *Opn5*) and neurokinin B (encoded by *Tacr3*). Consequently, we sought to determine whether the neurons responsible for inducing synthetic torpor in the rat share similarities to this torpor-inducing population identified in mice. We again used ISH to assess colocalization of virally transduced *mCherry* expression with three markers of QPLOT neurons, including *Ptger3*, *Lepr*, and *Opn5*. We found 100% of the virally transduced cells expressing *mCherry* also co-expressed *Ptger3* (Figure 2D-E). Additionally, 34% of these *mCherry* & *Ptger3* positive neurons also expressed *Opn5*, 18% co-expressed *LepR* (figure 2E), and 29% of *mCherry* positive neurons were positive for all three QPLOT neuron markers (figure 2E).

Induction of synthetic torpor protects the heart from ischaemia-reperfusion injury

Both hypothermia[38] and torpor[13,19,20] protect against ischaemia-reperfusion injury. We therefore sought to test the effects of synthetic torpor on tolerance to cardiac ischaemia-reperfusion injury in the ex-vivo Langendorff isolated heart preparation[39] (Figure 3A). Induction of synthetic torpor, 90 minutes prior to removal of the heart for the Langendorff preparation, reduced infarct by 39.5% (percentage infarcted myocardium: MPA^{Gq} 18.7 ± 9.6% vs MPA^{EGFP} 30.9 ± 9.1%, p <0.05, Figure 3B & C). It should be noted that although the synthetic torpor state reduced the body temperature of the rats prior heart excision, the perfusion of warm Krebs-Henseleit Buffer (KHB) to the tissue for a 30 minutes stabilisation period ensured that there were no differences in temperature at the time of ischaemia and reperfusion.

To examine whether the myocardial protection depends upon the preceding hypothermic effect of synthetic torpor we housed groups of MPA^{Gq} and MPA^{EGFP} rats at a thermoneutral temperature of 30°C when they were administered CNO. Administration of CNO to MPA^{Gq} rats housed at 30°C (thermoneutral conditions) prevented the drop in core temperature that was observed in recordings at room temperature (p <0.0001, see Figure 3D and Supplementary Figure 1A). Similarly in comparing thermoneutral MPA^{Gq} rats with thermoneutral MPA^{EGFP} control rats showed the expected fall in temperature was absent (mean temperature post-CNO in MPA^{Gq} rats 36.4 ± 0.73°C vs MPA^{EGFP} 37.05 ± 0.43°C, p =0.44, Figure 3D). However, the bradycardia observed in the rats housed at room temperature persisted even when rats were housed at a thermoneutral ambient temperature of 30°C (Figure 3E). A 21% lower heart rate was observed in the thermoneutral MPA^{Gq} compared to MPA^{EGFP} rats (mean heart rate post-CNO in thermoneutral MPA^{Gq} rats 298 ± 43 bpm vs thermoneutral MPA^{EGFP} rats 379 ± 62 bpm, p <0.05, see figure 3E and supplementary figure 1B). This indicates that the heart rate changes were not secondary to hypothermia. Additionally, there were no significant differences in the heart rate of animals in the MPA^{EGFP} condition compared to the thermoneutral MPA^{EGFP} condition (p = 0.53, Figure 3E) or between the MPA^{Gq} and thermoneutral MPA^{Gq} condition (p = 0.38, Figure 3E and Supplementary Figure 1B).

We found that thermoneutral synthetic torpor still significantly reduced the infarct size (percentage infarct in the thermoneutral MPA^{Gq} rats 9.6 ± 8.4 % compared to thermoneutral MPA^{EGFP} rats 36.2 ± 23.5 %, p <0.01, Figure 3C). There were no significant differences in infarct size between the MPA^{Gq} and thermoneutral MPA^{Gq} groups, (p = 0.31) nor between the MPA^{EGFP} and thermoneutral MPA^{EGFP} groups, (p = 0.38) (Figure 3C).

To test for the possibility that the bradycardia observed in-vivo during synthetic torpor persisted in the ex-vivo cardiac preparation, heart rate was measured during the Langendorf assay. No differences were observed in hearts rates during the 30-minute equilibration period (prior to induction of ischaemia) in MPA^{Gq} (240 ± 28 bpm), MPA^{EGFP} (248 ± 23 bpm), thermoneutral MPA^{Gq} (225 ± 20 bpm) and thermoneutral MPA^{EGFP} (225 ± 21 bpm) conditions, $F(3,19) = 1.35$, p = 0.29 (Supplementary Figure 1C).

This indicates the decreased heart rate observed during synthetic torpor in-vivo does not persist ex-vivo.

Mapping the distribution of the neurons responsible for synthetic torpor in the rat

We mapped the location of mCherry-expressing transduced neurons within the anterior hypothalamus. We observed transduced neurons in a region stretching from bregma +0.12mm to -0.48mm, spreading 1mm bilaterally from the midline, and from the ventral surface of the hypothalamus to 1.5mm dorsally (Figure 4). This region includes the targeted MPA as well as more caudal regions of the preoptic area such as the medial preoptic nucleus.

Discussion:

We utilised a chemogenetic model of synthetic torpor in the rat[40], a species that does not naturally enter torpor. We did this by targeting a population of hypothalamic neurons that correspond to those that drive natural fasting-induced torpor in the mouse. We demonstrate that synthetic torpor in the rat is cardioprotective in an ex-vivo ischemia-reperfusion injury model, even in the absence of hypothermia. Importantly, as synthetic torpor was induced in a species that does not naturally enter torpor, this work supports the hypothesis that the approach could be refined and translated for clinical use in humans.

Animals that were pre-conditioned with 90 minutes of synthetic torpor showed a 40% smaller infarct size compared to control animals (Figure 3). These findings support prior studies in species known to naturally enter torpor. For example: seasonal hibernators in torpor are highly tolerant of ischemia-reperfusion injury in multiple organs, including kidney and intestines[41–44]; inducing a torpor-like state using deep brain stimulation (DBS) to stimulate the medial preoptic area in mice is neuroprotective in a brain ischaemia model; and targeting RFP-amide expressing neurons in the MPA to trigger a torpor-like state ameliorates acute kidney injury[45,46] following ischaemia-reperfusion. Until now, this work was all carried out in species known to naturally enter torpor, including mice and ground squirrels, and so it was not clear whether other species might also benefit from an induced torpor-like state. Our study demonstrates for the first time that inducing a torpor-like state in a species that does not naturally enter torpor is protective in a cardiac ischemia-reperfusion injury model.

This study utilized an ex-vivo model of ischaemia-reperfusion injury, the Langendorff preparation. Our finding that activation of MPA EP3-expressing neurons in the rat was cardioprotective indicates that activity in this neuronal population induces changes in the cardiomyocytes that persist when the heart is isolated from the rest of the organism. Whether the protective signal in-vivo is circulating or released locally via vagal efferents remains an important question. The bradycardia we observed in-vivo in response to chemoactivation of neurons within the MPA still occurs in the absence of hypothermia (Figure 3E and Supplementary Figure 1B), suggesting active suppression of heart rate via the cardiac vagus nerve. Importantly, bradycardia did not persist during the ex-vivo Langendorff preparation (Supplementary Figure 1C). This was important to assess, as lower heart rate in the Langendorff assay has previously been shown to decrease the size of the infarcted tissue area[47]. Hence, our model of synthetic torpor appears to engage protective responses that persist in isolation and are neither temperature-dependent, nor driven by a simple reduction in the heart rate during ischaemia-reperfusion.

Strikingly, we also demonstrate that this cardioprotection induced by synthetic torpor persisted in the absence of hypothermia preceding the ex-vivo Langendorff preparation. This was established by the thermoneutral condition, which prevented the decrease in core body temperature while the animals were in synthetic torpor (Figure 3D) and resulted in a significant decrease in myocardial infarction size compared to thermoneutral control (Figure 3C). These data show that the hypothermic component of torpor is not necessary for the protective effects of synthetic torpor. There have so far been mixed

findings regarding the necessity for a drop in temperature to observe protection. One study used deep brain stimulation or chemogenetics to activate neurons within the mouse MPA to drive a torpor-like state and found that hypothermia is required for neuroprotection in a stroke model[45]. In contrast, and similar to our present study, Kyo and colleagues demonstrated that the hypothermic element of a torpor-like state in the mouse is not required for reducing acute kidney injury in response ischaemia[46]. Torpor-induced reduction in core temperature might be sufficient to improve tolerance to ischaemia-reperfusion injury, but some models (our present study and that of Kyo et al[46]) might engage additional, temperature-independent protective responses, or else they might engage the same end-organ process through additional temperature-independent mechanisms.

Recent years has seen a resurgence of interest in torpor and torpor-like states, driven by a hope that aspects of this remarkable physiology could be mimicked in both clinical and space-flight situations. Here we demonstrate that chemogenetic activation of neurons in the MPA of a non-hibernating species, the rat, was able to recapitulate three main features of natural torpor: hypothermia (Figure 1B), bradycardia (Figure 1C) and reduced oxygen consumption (Figure 1D). Taken together, our data supports the hypothesis that conserved mechanisms for entering a torpor-like state exist, even in species that do not naturally enter torpor, which may potentially be translated into humans.

The preoptic area of the hypothalamus (POA) is a key centre for control of energy balance, body temperature, and as a driver of natural fasting-induced torpor in the mouse[31,40,48,49]. Analysis of pooled single-nucleus RNA sequencing data has attempted to phenotype the critical neuronal population, from which emerge 'QPLOT neurons'[31,37,50]. These cells express QRFP[40], prostaglandins E3 receptor (EP3)[51], leptin receptor[52], the violet light sensitive receptor Opn5[53], and neurokinin 3 receptors (coded for by *Tacr3*)[54]. Expression of two or more of these markers is considered sufficient to identify neurons from this population[55]. 81% of the neurons we targeted with the DREADD viral vector expressed either two or three of these QPLOT neuron markers (Figure 2D-E). And 29% of these neurons expressed all three markers used, which included *Ptger3, Lepr* and *Opn5* (Figure 2D-E). The observation that virally transduced cells in the rat MPA also express QPLOT markers indicates that a population of neurons with equivalent expression patterns and physiological effects also exist in rats as well as in mice so are conserved across species.

We found that 72% of transduced mCherry neurons were positive for *Vglut2*, a marker of excitatory neurons (Figure 2B-C). Of these neurons, 37% were positive for *Vglut2* (Figure 2C), suggesting they are excitatory. 35% of transduced neurons were labelled as hybrid, expressing markers of both excitatory and inhibitory neurons (*Vglut2* and *Vgat*, Figure 2B-C). This was anticipated, as we used viral vector-mediated chemogenetics under the control of the CamKIIα promoter, which targets excitatory neurons[56,57]. Furthermore, a subset of neurons involved in mouse torpor, express both excitatory and inhibitory RNA markers[40]. Whether these neurons are functionally hybrid remains to be seen, but evidence in the rat suggests that while EP3 receptor-expressing thermoregulatory neurons in the preoptic area may express excitatory and inhibitory markers, they are functionally inhibitory[58].

A key question that emerges from the observation of synthetic torpor in the rat is: what is the natural role of these neural circuits and why do they not naturally induce torpor in response to fasting? EP3 receptor expressing neurons in the rat POA have been implicated in bidirectional control of body temperature[58]. These neurons are inhibited by prostaglandins to produce fever and activated by warmth exposure to reduce body temperature. It is highly likely that these neurons and the population we have identified overlap. Hence, rats might maintain the capacity to activate these neurons in response to rising ambient temperature, but no longer be able to activate them in response to fasting. Alternatively, the rat may engage these neurons to reduce temperature at sleep onset[59], but may have lost the ability to engage them to the extent that the animal enters torpor. Evidence that torpor and sleep are functionally linked comes from the observation that the medial preoptic area of the

hypothalamus appears to be responsible for triggering natural torpor[30,31,48] as well as the cooling associated with NREM sleep onset[25,26].

Our study represents an important step in the study of torpor and synthetic torpor states for clinical translation. We have shown that species that do not naturally enter torpor can be induced to do so through targeted activation of neuronal populations that correspond to those responsible for natural torpor in the mouse. This state of synthetic torpor confers protection from ischaemia-reperfusion independent of body temperature or heart rate, and which persists in the isolated heart. It adds to a growing body of evidence that the central nervous system is able to induce protective adaptations in the heart[60–62].

Methods:

Rats

All studies had the approval of the local University of Bristol Animal Welfare and Ethical Review Board and were conducted in accordance with the UK animals (scientific procedures) act. Male and female Wistar rats were obtained from Charles River, and were housed at 21°C on a 12-hour light/dark cycle with ad lib access to food and standard rat chow (LabDiet).

Viral vectors

AAV-CaMKIIa-hM3D(Gq)-mCherry was a gift from Bryan Roth (Addgene viral prep # 50476-AAV5) and was used at a titre of 1.7×10^{13} viral genome copies per ml. AAV-CaMKIIa-EGFP also a gift from Bryan Roth (Addgene viral prep # 50469-AAV5) and was used at a titre of 2.8×10^{13} viral genome copies per ml.

Stereotaxic injection of viral vectors

Rats were anaesthetised with intraperitoneal injection of ketamine (5mg/100g, Vetalar; Pharmacia) and medetomidine (30µg/100g Domitor, Pfizer) until loss of paw withdrawal reflex. Additional intraperitoneal injections of anaesthetic were administered as needed to maintain surgical depth of anaesthesia. Core temperature was maintained using a servo-controlled heat pad and a rectal temperature probe (Harvard Apparatus). The planned incision site was shaved, and skin cleaned with iodine solution and sterile surgical technique was used throughout. Anesthetized rats were placed in a stereotaxic frame, the head was fixed in atraumatic ear bars, and skull position maintained horizontal by an incisor bar (David Kopf Instruments). Microcapillary pipettes were made from microcapillary glass (Sigma) on a vertical pipette puller (Harvard Apparatus). Pipettes were filled with mineral oil; then vector was back-filled using a robotic microinjector (Nano-W wireless capillary microinjector, Neurostar), producing a visible vector–mineral oil interface. The scalp was incised in the midline and burr holes made bilaterally with a drill attachment (Neurostar). Bilateral injections were made at depths of 8.5mm relative to the surface of the brain, +0.12mm from Bregma and 0.4mm from the midline. Each injection was 200nl and was delivered at a rate of 100nl/minute. The injection pipette remained in place for 5 minutes after the injection before slowly removing. Following vector injections, the wound was closed with nonabsorbable suture and dressed with antibacterial wound powder. Anaesthesia was reversed with atipamezole (1 mg/kg i.p, Antisedan, Zoetis), and meloxicam analgesia given subcutaneously (5mg/kg, Metacam, Boehringer Ingelheim). Rats were recovered in a heated chamber, then housed separately for three days following surgery and monitored daily.

Implantation of telemeters

During the anaesthesia for stereotaxic CNS injections, a subset of rats was additionally implanted with telemetric temperature and electrocardiogram (ECG) probes into the abdomen (DSI ETA-F10 implant, Data Science International, Harvard Bioscience Inc). A vertical incision was made through the skin in the abdomen just below the sternum approximately 2-3 cm in length and a smaller incision made to the skin at the right hand side of the chest, for placement of the ECG electrode. Telemeter wires were

passed under the skin and sewn into place using non-absorbable sutures. An intraperitoneal incision was made into the abdomen for placement of the telemetry implant, which was closed with absorbable sutures. Finally, the skin incisions were closed with non-absorbable sutures and dressed with antibacterial wound powder. Anaesthesia was reversed with atipamezole (1 mg/kg i.p, Antisedan, Zoetis), and meloxicam analgesia given subcutaneously (5mg/kg, Metacam, Boehringer Ingelheim). Rats were recovered in a heated chamber, then housed separately for three days following surgery and monitored daily.

Induction of synthetic torpor

Intraperitoneal injection of clozapine-N-oxide dihydrochloride (CNO), a synthetic ligand that activates the DREADD $hM3D_q$ (2 mg/kg, Tocris Bioscience, #6329), was used to induce synthetic torpor. For those rats that were not implanted with telemeters, synthetic torpor induction was confirmed using thermal imaging with a Flir C2 camera. Synthetic torpor was defined by a drop in core temperature below 35°C in telemetered animals, or surface temperature below 30°C in thermally imaged animals following CNO injection.

Telemetric monitoring of core body temperature, ECG and motor activity

Telemetry implants were switched on and connected to a receiver platform (DSI PhysioTel™ receiver RPC-1, Data Science International, Harvard Bioscience Inc). Continuous telemetry data, including core body temperature, ECG and motor activity were acquired and recorded wirelessly using DSI Matrix 2.0 (MX2, Data Science International, Harvard Bioscience Inc) and Ponemah software (Ponemah v6.00, Data Science International, Harvard Bioscience Inc). Recordings were made from animals in their home cages for data at room temperature. For the thermoneutral condition, recordings were made from animals habituated to a heated chamber that was maintained at 28°C (controls) or 30°C (synthetic torpor). Post-recording, ECG, temperature and activity data were filtered to remove noise and analysed in Ponemah software. The R wave component of the ECG recordings was detected and used to determine the heart rate in bpm.

Measurement of oxygen consumption

Indirect calorimetry was performed using a CaloBox (Phenosys)[63], with a gas flow rate of 75 litres per hour and a sampling rate of 0.25Hz. Rats were first acclimated to the recording chamber before undergoing CNO injection. Food and drink were available throughout the recording session.

Ex-vivo model of cardiac ischemia-reperfusion injury

90 min post CNO administration, an intraperitoneal injection of heparin was delivered (1,000 IU, Sigma-Aldrich, #H3393) to avoid thrombus formation. Animals were deeply anesthetized with isoflurane (5%) which was delivered in a constant flow of oxygen (2 l/min). Following loss of pedal reflex, animals were sacrificed by cervical dislocation. A thoracotomy was performed and beating hearts were removed by sectioning the aorta. Hearts were quickly placed into ice-cold Krebs-Henseleit Buffer (KHB) (containing 120 mM NaCl, 25 mM $NaHCO_3$, 11 mM Glucose, 1.2 mM KH_2PO_4, 1.2 mM $MgSO_4$, 4.8 mM KCl and 1.2 mM $CaCl_2$). The aorta was then cannulated (secured into place using suture threads) and hearts were perfused by the Langendorff method (Langendorff, 1898) on an isolated heart system apparatus. Hearts were perfused with carbonated KHB, maintained at 37°C, at a rate of 10 ml/min. ECG was continuously recorded by Ag electrodes placed near the apex of the heart. After a 30-minute stabilization phase, the hearts were then subjected to 30 minutes of global ischemia, whereby perfusion was stopped, and hearts were submerged into a water-jacketed bath of KHB held at 37°C. After ischemia, the hearts were reperfused for 60 minutes (figure 2A). Exclusion criteria for experiments included excessive time between excision of the heart and start of *ex-vivo* perfusion with KHB of more than 2 minutes, more than 2 aortic cannulation attempts, and heart rate under 200 bpm at the end of the equilibration period.

Heart infarction assessment

Following 60 minutes of reperfusion, the hearts were perfused with 2.3.5-Triphenyltetrazolium Chloride (TTC) (Phytotech, USA) to demarcate infarcted tissue (unstained by TTC) and viable tissue (stained by TTC)[64]. 1% TTC solution at 37°C was perfused through the aortic cannula at a rate of 2 ml/min and then hearts were submerged in 1% TTC for a further 15 mins at 37°C, before being fixed in 4% paraformaldehyde for 24 hours at 4°C. Hearts were then transversally sliced into 3 mm thick sections and each side of the sections were imaged using a flatbed scanner. ImageJ (NIH, USA) was used to outline and calculate the infarcted area and whole heart area (excluding ventricular chambers). Both infarcted and viable areas were averaged across each side for each heart section and infarct area was expressed as a percentage dividing total infarcted area by whole heart area. The assessor was blinded to the animal group.

Mapping of virally transfected MPA hypothalamic neurons:

Immunofluorescence

Brains were extracted and post-fixed for 48 hours with 4% PFA at 4°C and then incubated in PBS with 30% sucrose and 0.03% sodium azide for a further 48 hours. Brains were embedded in tissue freezing medium and sectioned on a freezing microtome into 40 µm coronal sections and adhered to SuperFrost Plus slides (Epredia). A hydrophobic barrier was drawn around each slide using an ImmEdge Pen (Vector Laboratories) and allowed to dry at room temperature for 15 min. Sections were washed 3 times for 5 min in PBS and then blocked with 0.25% Bovine Serum Albumin (BSA) and 10% Normal Donkey Serum (NDS) in 0.3% Triton-X PBS (PBS-T) for 4 hours at room temperature. They were then incubated with primary antibody (anti-mCherry, 1:2000 dilution, BioVision, #5993) diluted in 0.25% BSA and 2% NDS in PBS-T overnight at room temperature. Slides were then washed 3 times for 5 min in PBS, followed by incubation with the secondary antibody (Alexa Fluor 594 donkey anti-rabbit, 1:1000 dilution, Abcam, #A-21207) diluted in 0.25% BSA in PBS-T for 4 hours at room temperature. Finally, slides were washed 3 times for 5 min in PBS and mounted with Fluoroshield with DAPI (Sigma Aldrich).

Epifluorescence imaging & mapping

Sections were imaged using a Leica DM4000B widefield microscope with a 20x magnification 0.5 numerical aperture objective, with a 515-561nm excitation filter, dichroic mirror 580nm, and a 590nm emission filter. The anatomical extent of virally transduced cells was mapped independently by two individuals and agreed by consensus using the Allen brain atlas as reference.

Characterisation of neurons driving this torpor-like state:

Fluorescence in situ hybridization (ISH)

Brains were extracted and immediately frozen in 2-methylbutane and stored at -80°C until use. Brains were embedded in tissue freezing medium (Cryomatrix™, ThermoFisher) and sliced on a cryostat into 20µm coronal sections, adhered to SuperFrost Plus slides (Epredia) and stored at -20°C overnight before undergoing the standard RNAscope Fluorescent Multiplex Assay for fresh frozen tissue (ACD Bio, Biotechne).

For the RNAscope ISH, mounted sections were fixed in 4% PFA for 15 min at room temperature, then dehydrated in increasing concentrations of ethanol (50%, 75%, then 100%) for 5 minutes in each. Sections were left overnight in a 2nd application of 100% ethanol. 2 sections per animal were selected for processing based on mCherry expression within the MPA and underwent 1 of 2 protocols, protocol 1: markers of excitatory and inhibitory neurons, and Protocol 2: markers that have been associated with neurons controlling mouse torpor (see table 1 for probes used). Dehydrated sections were air-dried for 10 min at room temperature, treated with hydrogen peroxide for 10 minutes at room temperature, washed with distilled water and then treated with protease IV for 12 min. The RNAscope probes were then applied to each slide and left to hybridize for 2 h at 40°C in a humidified chamber. Following hybridization, slides were washed with wash buffer twice for 2 minutes at room

409 temperature. AMP1 was applied to each slide and left to incubate in a humidified oven for 30 minutes
410 at 40°C, then washed again twice for 2 minutes. This amplification process was repeated for AMP2 and
411 AMP3. Next, slides were washed twice with wash buffer for 2 minutes at room temperature and HRP-
412 C1 was applied to sections for 15 minutes at 40°C in a humidified chamber. Slides were rinsed again
413 with wash buffer for 2 minutes at room temperature and an Opal dye was incubated on the slides for
414 30 minutes at 40°C in a humidified chamber. Following this, slides were washed with wash buffer for
415 2 minutes at room temperature and the HRP blocker was applied to sections for 15 minutes at 40°C in
416 a humidified chamber. This process was repeated for HRP-C2, C3 and C4 with different Opal dyes for
417 each. Finally, the sections were rinsed in wash buffer for 2 minutes at room temperature and
418 coverslipped with fluoroshield with DAPI and left to dry at room temperature overnight, before being
419 stored at 4°C.
420

Target	Protocol	Gene (entrez gene ID)	Species (homology*)	*Catalogue number (Channel)*
VGLUT2	*1*	*Slc17a6 (84487)*	*Rat*	*317011 (C4)*
VGAT	*1*	*Slc32a1 (22348)*	*Mouse (97.6%)*	*319191 (C1)*
Prostaglandin E2 receptor (EP3)	*2*	*Ptger3 (249290)*	*Rat*	*586251 (C4)*
Leptin receptor	*2*	*LepR (24536)*	*Rat*	*415951 (C2)*
Opn5 receptor	*2*	*Opn5 (353344)*	*Mouse (96.4%)*	*438071 (C1)*
mCherry	*1 & 2*	*mCherry*	*n/a*	*431201 (C3)*

421 Table 1: RNAscope probes used for ISH. *https://rddc.tsinghua-gd.org/
422
423 *Confocal imaging*
424 Brains were processed as indicated in *Fluorescence in situ hybridization* section and imaged within 2
425 weeks of processing. Sections containing MPA were imaged on a Leica SP8 AOBS confocal laser
426 scanning microscope attached to a Leica DMi8 inverted epifluorescence microscope using HyD
427 detectors ("hybrid" SMD GaAsP detectors) with 405 nm diode and white light lasers. A 40x oil
428 immersion lens with NA of 1.3 (HC PL APO CS2 lens). Tiled MPA images were taken and stitched using
429 LASX software (Leica) and channels were imaged sequentially to avoid optical crosstalk.
430
431 *In situ hybridization image analysis*
432 Images were z projection compressed in ImageJ. A 50-pixel radius rolling ball background subtraction
433 was applied to each image. An automated image processing pipeline was used to count DAPI- and
434 RNA- positive nuclei. An Otsu threshold was applied to the DAPI image and overlapping nuclei were
435 separated using the watershed method. Cell nuclei were then filtered by size (20-200μm^2) and counted
436 and ROIs for each cell nuclei were saved in ImageJ. ROIs and cell identities created from the DAPI image
437 were then overlayed on the ISH images and cell nuclei positive for RNA were counted. A minimum of
438 200 cells from each brain section were manually assessed to determine a threshold for nuclei positive
439 for the different RNA transcripts and these thresholds were then applied to the remaining cells.
440
441 *Statistical analysis*
442 Descriptive statistics including mean ± standard deviations are reported in the main text. Statistical
443 details for experiments can be found in figure legends, including n numbers, statistical test used and
444 level of significance. One-way analysis of variance (ANOVA) was used for multiple group comparisons,
445 followed by Sidak's or Holm-Sidak's post hoc test to identify significant differences as reported in the
446 text and figure legends. A paired t-test was used to analyse the oxygen consumption data. All analyses
447 were performed in GraphPad Prism (Version 10.4.1).

448 **Figures**

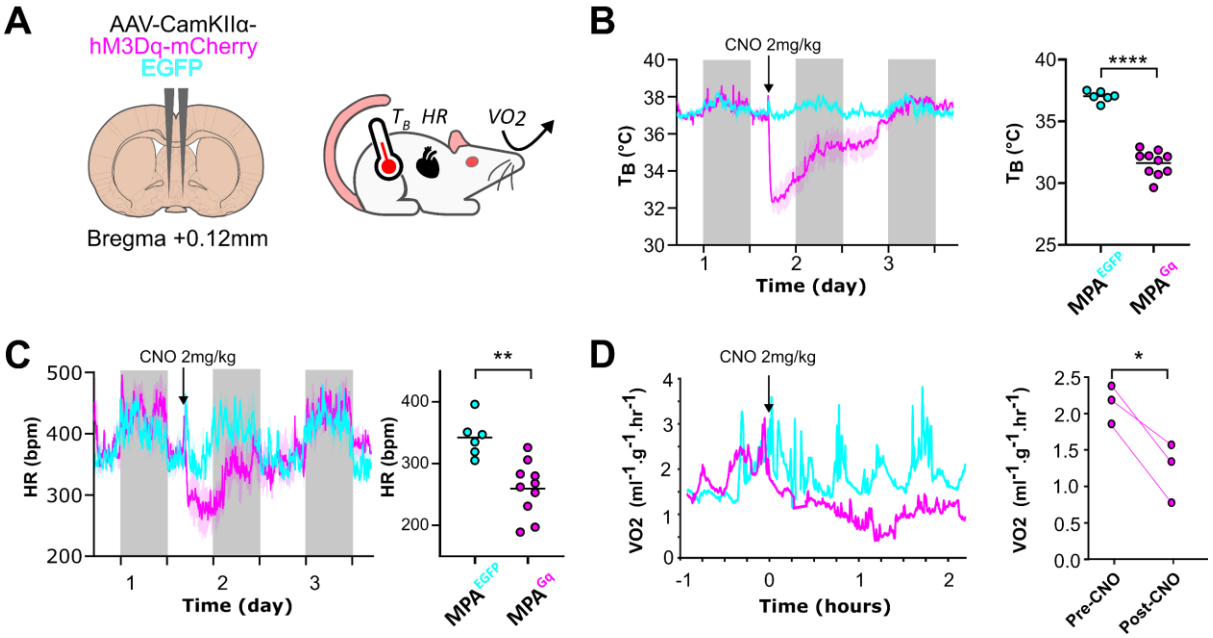

449

450 **Figure 1. Chemogenetic activation of neurons in the rat medial preoptic area (MPA, A) induces**
451 **synthetic torpor** characterised by reduced core body temperature (B, F(3,24) = 106.4. $p < 0.0001$),
452 bradycardia (C, F(3,24) = 9.637, $p = 0.0002$), and reduced oxygen consumption (D, t(2) = 6.15, $P =$
453 0.026). For B and C, $n = 4$ controls and 5 synthetic torpor, mean value for 10 minutes 90 minutes after
454 CNO 2mg/kg IP. For D, $n = 3$ synthetic torpor pre- vs post CNO. Shaded area indicates S.E.M. * indicates
455 $p < 0.05$, ** indicates $p < 0.01$, *** indicates $p < 0.001$, **** indicates $p < 0.0001$. Abbreviations: T_B,
456 core temperature; VO_2, oxygen consumption; HR, heart rate; CNO, clozapine-N-oxide; ST, synthetic
457 torpor; bpm, beats per minute.

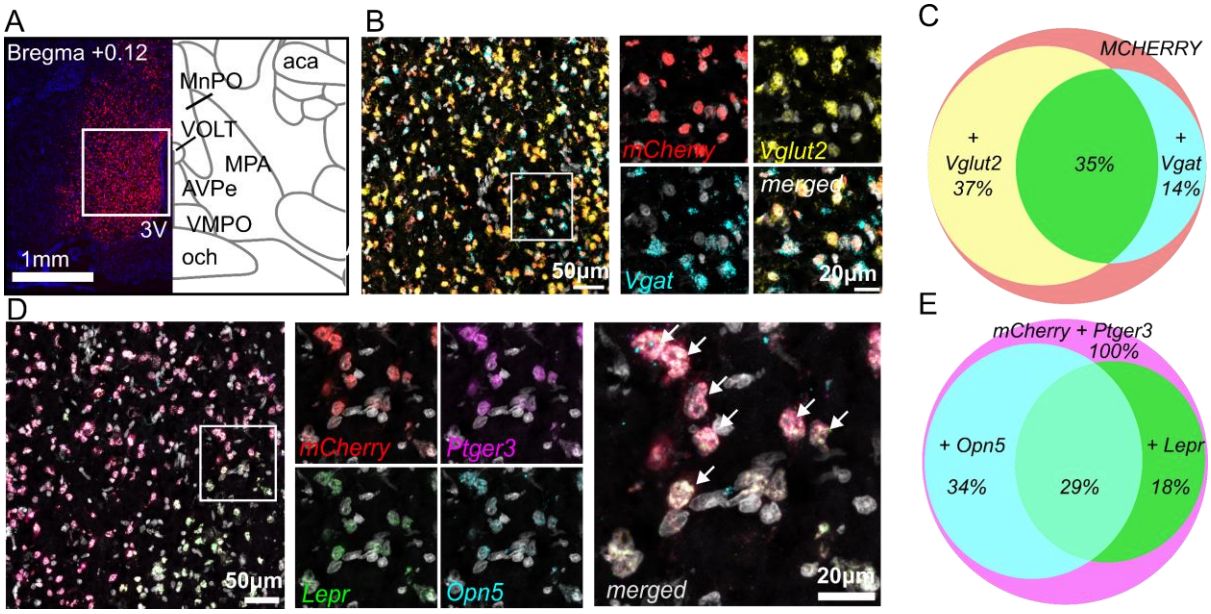

Figure 2. Characterisation of neurons in the rat MPA responsible for inducing synthetic torpor. A, viral transduction in the MPA (red) and corresponding anatomical schematic. B, RNA *in-situ* hybridisation labelling virally transduced cells (*mCherry*, red), and those expressing *Vglut2* (yellow) and/or *Vgat* (turquoise). C, expression of *Vglut2* and *Vgat* amongst transduced cells. D, RNA *in-situ* hybridisation labelling virally transduced cells (*mCherry*, red), and those expressing *Ptger3* (purple), *Lepr* (green), and/or *Opn5* (turquoise). White arrows indicate transduced cells that express *Ptger3*, *Lepr*, and *Opn5*. E, expression of QPLOT markers amongst virally transduced cells (note all transduced cells expressed *Ptger3*). Abbreviations: MnPO, median preoptic nucleus; VOLT, vascular organ of the lamina terminalis; 3V, third ventricle; AVPe, anteroventral periventricular nucleus; VMPO, ventromedial preoptic nucleus; och, optic chiasm; MPA, medial preoptic area; aca, anterior commissure (anterior part); *Vglut2*, vesicular glutamate transporter 2; *Vgat*, vesicular GABA transporter; *Ptger3*, prostaglandin EP3 receptor; *Lepr*, leptin receptor; *Opn5*, opsin-5.

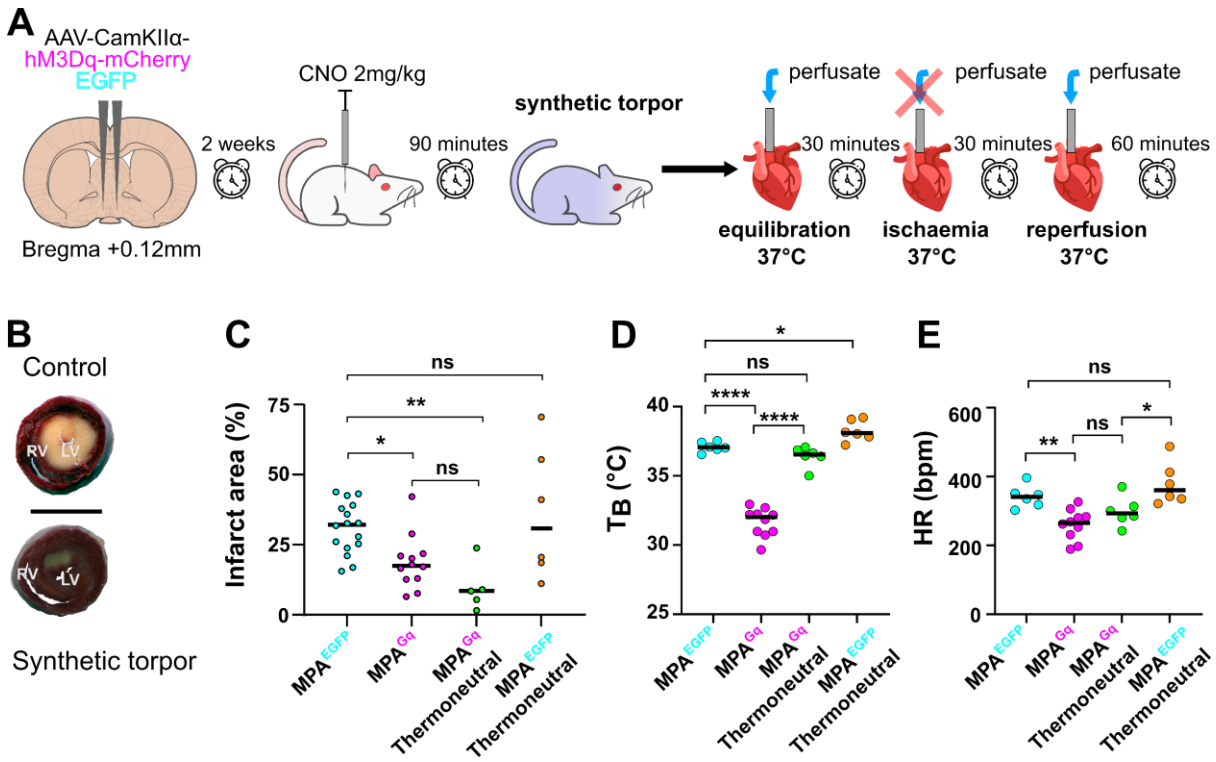

Figure 3. Synthetic torpor protects the heart from ex-vivo ischaemia-reperfusion injury model. Rats first underwent bilateral injection of vector (hM3DGq or GFP) into the MPA. After two weeks, they received CNO, to induce synthetic torpor in rats that had received hM3DGq vector, followed by removal of the heart and ischaemia-reperfusion (A). Pre-conditioning with synthetic torpor resulted in significantly reduced infarct size as measured by 2.3.5-Triphenyltetrazolium Chloride (TTC) staining (B, C). Scale bar represents 1cm). This cardioprotective effect was not dependent on a reduction in core temperature as rats held at a thermoneutral ambient temperature following CNO injection were still protected (C, ANOVA F (3,35) = 6.542, p = 0.0013). Inducing synthetic torpor in a thermoneutral environment prevented the drop in core temperature (D, F(3,24) = 106.4. P < 0.0001), but not the bradycardia (E, F(3,24) = 9.637, p = 0.0002,). Holm-Sidak correction used throughout for multiple comparisons. Data shown is median and IQR. * indicates p <0.05, ** indicates p < 0.01, **** indicates p < 0.00001, ns indicates p >0.05. Abbreviations: CNO, clozapine-N-oxide; ST, synthetic torpor; RV, right ventricle; LV, left ventricle; T_B, core temperature; HR, heart rate; bpm, beats per minute.

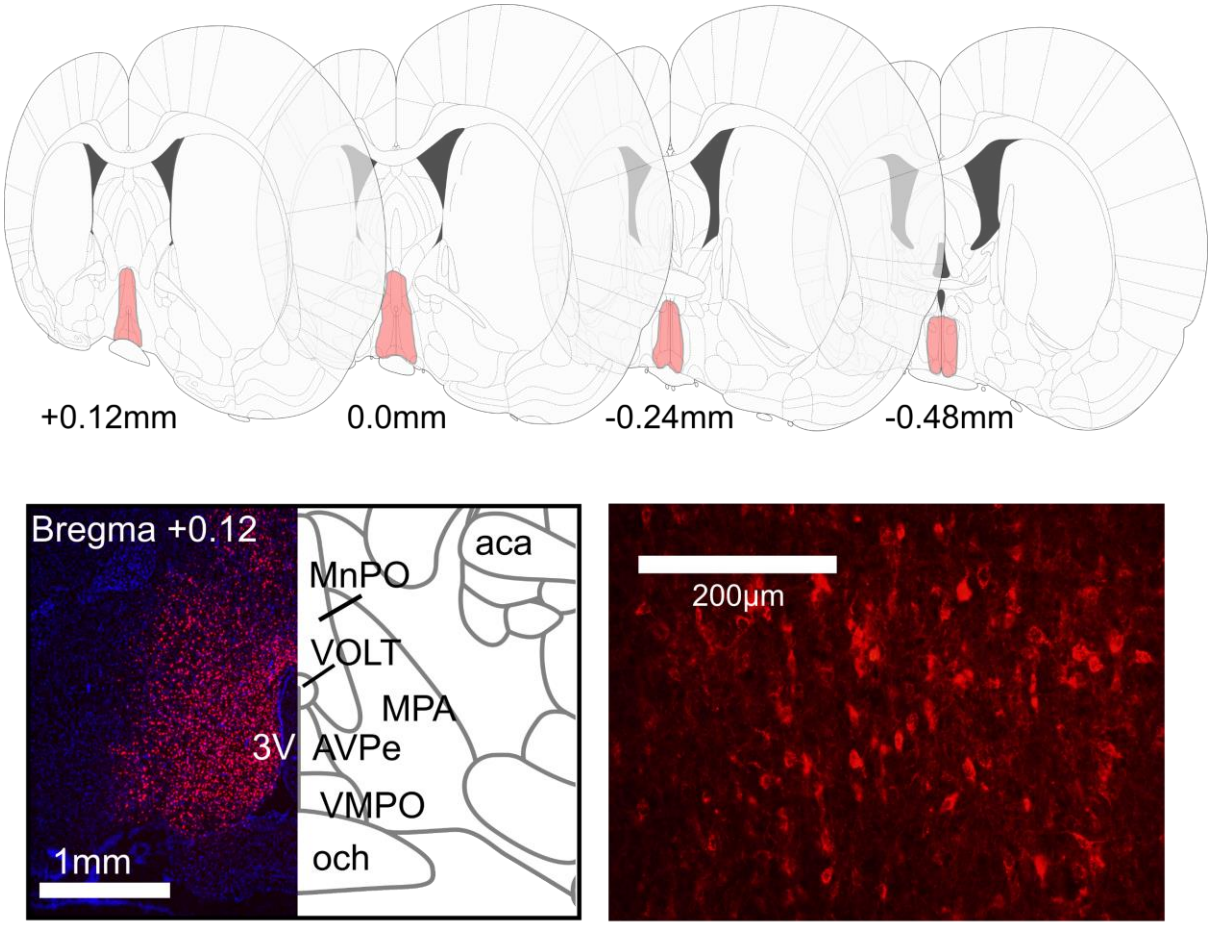

Figure 4. Distribution of neurons responsible for inducing synthetic torpor. A, schematic showing extent of viral transduction common to all animals. B & C, injection target site showing transduced neurons (red) and corresponding anatomical regions. Abbreviations: MnPO, median preoptic nucleus; VOLT, vascular organ of the lamina terminalis; 3V, third ventricle; AVPe, anteroventral periventricular nucleus; VMPO, ventromedial preoptic nucleus; och, optic chiasm; MPA, medial preoptic area; aca, anterior commissure (anterior part).

496 **Supplementary figures:**

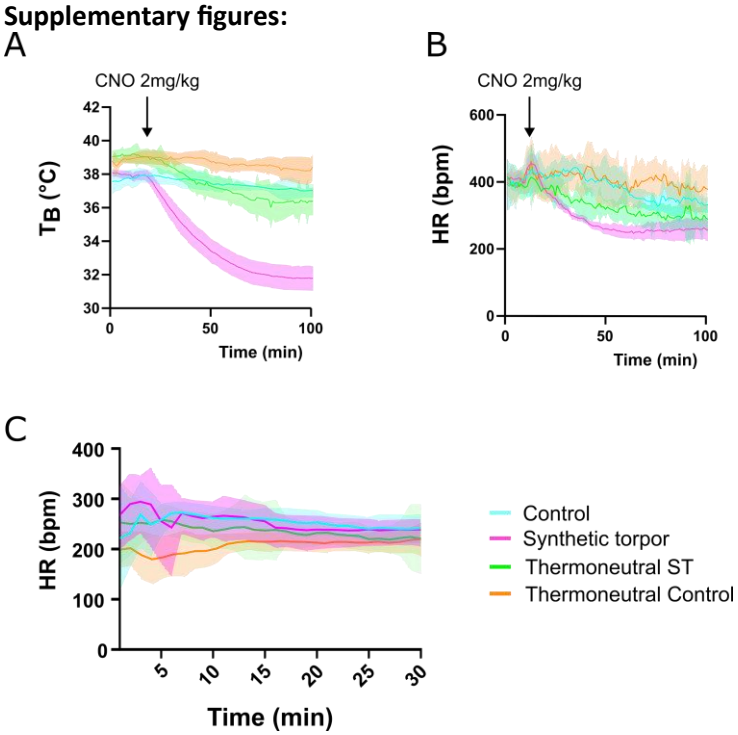

497
498

499 **Supplementary figure 1. Pre-Langendorff characteristics (A,B) and on-prep heart rates (C). Core**
500 **temperature (A) and heart rate (B) prior to excision of heart for Langendorff preparation.** A,B, n = 6
501 controls, 10 synthetic torpor, 6 thermoneutral synthetic torpor, & 6 thermoneutral controls. C, controls
502 (n = 16), torpor (n = 12), thermoneutral synthetic torpor (n = 5), & thermoneutral controls (n = 6). No
503 significant differences in on-prep HR were observed between the four groups during the 30-minute
504 equilibration period of the Langendorff assay ($F(3,19) = 1.35$, $p = 0.29$). Data shows mean and 95%
505 confidence interval. Abbreviations: ST, synthetic torpor; HR, heart rate; bpm, beats per minute.

506 **References**

507 1. Virani, S. S. *et al.* Heart Disease and Stroke Statistics—2021 Update: A Report From the American
508 Heart Association. *Circulation* **143**, (2021).
509 2. Murray, C. J. L. *et al.* Global burden of 87 risk factors in 204 countries and territories, 1990–2019:
510 a systematic analysis for the Global Burden of Disease Study 2019. *The Lancet* **396**, 1223–1249
511 (2020).
512 3. Zhang, M. *et al.* Ischemia-reperfusion injury: molecular mechanisms and therapeutic targets. *Sig*
513 *Transduct Target Ther* **9**, 12 (2024).
514 4. Van Der Worp, H. B., Macleod, M. R., Kollmar, R., & for the European Stroke Research Network for
515 Hypothermia (EuroHYP). Therapeutic Hypothermia for Acute Ischemic Stroke: Ready to Start Large
516 Randomized Trials? *J Cereb Blood Flow Metab* **30**, 1079–1093 (2010).
517 5. Leonov, Y. *et al.* Mild Cerebral Hypothermia during and after Cardiac Arrest Improves Neurologic
518 Outcome in Dogs. *J Cereb Blood Flow Metab* **10**, 57–70 (1990).
519 6. Chu, S.-J. *et al.* Effects of Various Body Temperatures After Lipopolysaccharide-Induced Lung Injury
520 in Rats. *Chest* **128**, 327–336 (2005).
521 7. Zhang, S. *et al.* Hypothermia evoked by stimulation of medial preoptic nucleus protects the brain
522 in a mouse model of ischaemia. *Nat Commun* **13**, 6890 (2022).
523 8. Kyo, S. *et al.* Quiescence-inducing neurons-induced hypometabolism ameliorates acute kidney
524 injury in a mouse model mimicking cardiovascular surgery requiring circulatory arrest. *JTCVS Open*
525 **12**, 201–210 (2022).
526 9. Nielsen, N. *et al.* Targeted Temperature Management at 33°C versus 36°C after Cardiac Arrest. *N*
527 *Engl J Med* **369**, 2197–2206 (2013).
528 10. Dankiewicz, J. *et al.* Hypothermia versus Normothermia after Out-of-Hospital Cardiac Arrest. *N*
529 *Engl J Med* **384**, 2283–2294 (2021).
530 11. Dundee, J. W., Gray, T. C., Mesham, P. R. & Scott, W. E. B. Hypothermia with Autonomic Block in
531 Man. *BMJ* **2**, 1237–1243 (1953).

532 12. Sandestig, A., Romner, B. & Grände, P.-O. Therapeutic Hypothermia in Children and Adults with
533 Severe Traumatic Brain Injury. *Therapeutic Hypothermia and Temperature Management* **4**, 10–20
534 (2014).
535 13. Zancanaro, C., Malatesta, M., Mannello, F., Vogel, P. & Fakan, S. The kidney during hibernation and
536 arousal from hibernation. A natural model of organ preservation during cold ischaemia and
537 reperfusion. *Nephrology Dialysis Transplantation* **14**, 1982–1990 (1999).
538 14. Bolling, S. F. *et al.* Use of "Natural" Hibernation Induction Triggers for Myocardial Protection. *The*
539 *Annals of Thoracic Surgery* **64**, 623–627 (1997).
540 15. Cerri, M. The Central Control of Energy Expenditure: Exploiting Torpor for Medical Applications.
541 *Annu. Rev. Physiol.* **79**, 167–186 (2017).
542 16. Ambler, M., Hitrec, T. & Pickering, A. Turn it off and on again: characteristics and control of torpor.
543 *Wellcome Open Res* **6**, 313 (2021).
544 17. Swoap, S. J. & Gutilla, M. J. Cardiovascular changes during daily torpor in the laboratory mouse.
545 *American Journal of Physiology-Regulatory, Integrative and Comparative Physiology* **297**, R769–
546 R774 (2009).
547 18. Heldmaier, G., Ortmann, S. & Elvert, R. Natural hypometabolism during hibernation and daily
548 torpor in mammals. *Respiratory Physiology & Neurobiology* **141**, 317–329 (2004).
549 19. Bhowmick, S., Moore, J. T., Kirschner, D. L. & Drew, K. L. Arctic ground squirrel hippocampus
550 tolerates oxygen glucose deprivation independent of hibernation season even when not
551 hibernating and after ATP depletion, acidosis, and glutamate efflux. *J. Neurochem.* **142**, 160–170
552 (2017).
553 20. Jani, A. *et al.* Renal Protection From Prolonged Cold Ischemia and Warm Reperfusion in
554 Hibernating Squirrels. *Transplantation* **92**, 1215–1221 (2011).
555 21. Barnes, E. B. M. & Carey, H. V. Evolution, Mechanisms, Adaptation, and Application.
556 22. Srere, H. K., Wang, L. C. & Martin, S. L. Central role for differential gene expression in mammalian
557 hibernation. *Proc. Natl. Acad. Sci. U.S.A.* **89**, 7119–7123 (1992).

23. Faherty, S. L., Villanueva-Cañas, J. L., Klopfer, P. H., Albà, M. M. & Yoder, A. D. Gene Expression Profiling in the Hibernating Primate, *Cheirogaleus Medius*. *Genome Biol Evol* **8**, 2413–2426 (2016).
24. Zhao, S. *et al.* Genomic analysis of expressed sequence tags in American black bear Ursus americanus. *BMC Genomics* **11**, 201 (2010).
25. Harding, E. C. *et al.* A Neuronal Hub Binding Sleep Initiation and Body Cooling in Response to a Warm External Stimulus. *Current Biology* **28**, 2263-2273.e4 (2018).
26. Zhang, Z. *et al.* Neuronal ensembles sufficient for recovery sleep and the sedative actions of α2 adrenergic agonists. *Nat Neurosci* **18**, 553–561 (2015).
27. Cerri, M. *et al.* The Inhibition of Neurons in the Central Nervous Pathways for Thermoregulatory Cold Defense Induces a Suspended Animation State in the Rat. *J. Neurosci.* **33**, 2984–2993 (2013).
28. Zakharova, N. M. *et al.* A pharmacological composition for induction of a reversible torpor-like state and hypothermia in rats. *Life Sciences* **219**, 190–198 (2019).
29. Ferhat, L. *et al.* A peptide-neurotensin conjugate that crosses the blood-brain barrier induces pharmacological hypothermia associated with anticonvulsant, neuroprotective and anti-inflammatory properties following status epilepticus in mice. *eLife* **13**, (2024).
30. Takahashi, T. M. *et al.* A discrete neuronal circuit induces a hibernation-like state in rodents. *Nature* **583**, 109–114 (2020).
31. Hrvatin, S. *et al.* Neurons that regulate mouse torpor. *Nature* **583**, 115–121 (2020).
32. Zhang, Z. *et al.* Estrogen-sensitive medial preoptic area neurons coordinate torpor in mice. *Nat Commun* **11**, 6378 (2020).
33. Armbruster, B. N., Li, X., Pausch, M. H., Herlitze, S. & Roth, B. L. Evolving the lock to fit the key to create a family of G protein-coupled receptors potently activated by an inert ligand. *Proc. Natl. Acad. Sci. U.S.A.* **104**, 5163–5168 (2007).
34. Roth, B. L. DREADDs for Neuroscientists. *Neuron* **89**, 683–694 (2016).
35. Basu, K. *et al.* Novel strategy to selectively label excitatory and inhibitory neurons in the cerebral cortex of mice. *Journal of Neuroscience Methods* **170**, 212–219 (2008).

584 36. Egashira, Y., Mori, Y., Yanagawa, Y. & Takamori, S. Development of lentiviral vectors for efficient
585 glutamatergic-selective gene expression in cultured hippocampal neurons. *Sci Rep* **8**, 15156
586 (2018).
587 37. Upton, B. A., D'Souza, S. P. & Lang, R. A. QPLOT Neurons—Converging on a Thermoregulatory
588 Preoptic Neuronal Population. *Front. Neurosci.* **15**, 665762 (2021).
589 38. Kuczynski, A., Demchuk, A. & Almekhlafi, M. Therapeutic hypothermia: Applications in adults with
590 acute ischemic stroke. *Brain Circ* **5**, 43 (2019).
591 39. Bell, R. M., Mocanu, M. M. & Yellon, D. M. Retrograde heart perfusion: The Langendorff technique
592 of isolated heart perfusion. *Journal of Molecular and Cellular Cardiology* **50**, 940–950 (2011).
593 40. Takahashi, T. M. *et al.* A discrete neuronal circuit induces a hibernation-like state in rodents. *Nature*
594 **583**, 109–114 (2020).
595 41. Zancanaro, C., Malatesta, M., Mannello, F., Vogel, P. & Fakan, S. The kidney during hibernation and
596 arousal from hibernation. A natural model of organ preservation during cold ischaemia and
597 reperfusion. *Nephrology Dialysis Transplantation* **14**, 1982–1990 (1999).
598 42. Bhowmick, S., Moore, J. T., Kirschner, D. L. & Drew, K. L. Arctic ground squirrel hippocampus
599 tolerates oxygen glucose deprivation independent of hibernation season even when not
600 hibernating and after ATP depletion, acidosis, and glutamate efflux. *J. Neurochem.* **142**, 160–170
601 (2017).
602 43. Jani, A. *et al.* Renal Protection From Prolonged Cold Ischemia and Warm Reperfusion in
603 Hibernating Squirrels. *Transplantation* **92**, 1215–1221 (2011).
604 44. Kurtz, C. C., Lindell, S. L., Mangino, M. J. & Carey, H. V. Hibernation confers resistance to intestinal
605 ischemia-reperfusion injury. *American Journal of Physiology-Gastrointestinal and Liver Physiology*
606 **291**, G895–G901 (2006).
607 45. Zhang, S. *et al.* Hypothermia evoked by stimulation of medial preoptic nucleus protects the brain
608 in a mouse model of ischaemia. *Nat Commun* **13**, 6890 (2022).

609 46. Kyo, S. *et al.* Quiescence-inducing neurons-induced hypometabolism ameliorates acute kidney
610 injury in a mouse model mimicking cardiovascular surgery requiring circulatory arrest. *JTCVS Open*
611 **12**, 201–210 (2022).
612 47. Delgado-Betancourt, V. *et al.* Heart rate reduction after genetic ablation of L-type Cav1.3 channels
613 induces cardioprotection against ischemia-reperfusion injury. *Front Cardiovasc Med* **10**, 1134503
614 (2023).
615 48. Ambler, M., Hitrec, T., Wilson, A., Cerri, M. & Pickering, A. Neurons in the Dorsomedial
616 Hypothalamus Promote, Prolong, and Deepen Torpor in the Mouse. *J. Neurosci.* **42**, 4267–4277
617 (2022).
618 49. Saper, C. B. & Machado, N. L. S. Flipping the switch on the body's thermoregulatory system. *Nature*
619 **583**, 34–35 (2020).
620 50. Moffitt, J. R. *et al.* Molecular, Spatial and Functional Single-Cell Profiling of the Hypothalamic
621 Preoptic Region. (2019).
622 51. Machado, N. L. S., Bandaru, S. S., Abbott, S. B. G. & Saper, C. B. EP3R-Expressing Glutamatergic
623 Preoptic Neurons Mediate Inflammatory Fever. *J. Neurosci.* **40**, 2573–2588 (2020).
624 52. Yu, S. *et al.* Glutamatergic Preoptic Area Neurons That Express Leptin Receptors Drive
625 Temperature-Dependent Body Weight Homeostasis. *J. Neurosci.* **36**, 5034–5046 (2016).
626 53. Zhang, K. X. *et al.* Violet-light suppression of thermogenesis by opsin 5 hypothalamic neurons.
627 *Nature* **585**, 420–425 (2020).
628 54. Padilla, S. L., Johnson, C. W., Barker, F. D., Patterson, M. A. & Palmiter, R. D. A Neural Circuit
629 Underlying the Generation of Hot Flushes. *Cell Reports* **24**, 271–277 (2018).
630 55. Upton, B. A., D'Souza, S. P. & Lang, R. A. QPLOT Neurons—Converging on a Thermoregulatory
631 Preoptic Neuronal Population. *Front. Neurosci.* **15**, 665762 (2021).
632 56. Basu, K. *et al.* Novel strategy to selectively label excitatory and inhibitory neurons in the cerebral
633 cortex of mice. *Journal of Neuroscience Methods* **170**, 212–219 (2008).

57. Egashira, Y., Mori, Y., Yanagawa, Y. & Takamori, S. Development of lentiviral vectors for efficient glutamatergic-selective gene expression in cultured hippocampal neurons. *Sci Rep* **8**, 15156 (2018).

58. Nakamura, Y. *et al.* Prostaglandin EP3 receptor–expressing preoptic neurons bidirectionally control body temperature via tonic GABAergic signaling. *SCIENCE ADVANCES* (2022).

59. Alföldi, P., Rubicsek, G., Cserni, G. & Obál, F. Brain and core temperatures and peripheral vasomotion during sleep and wakefulness at various ambient temperatures in the rat. *Pflugers Arch.* **417**, 336–341 (1990).

60. Haykin, H. *et al.* Reward system activation improves recovery from acute myocardial infarction. *Nat Cardiovasc Res* **3**, 841–856 (2024).

61. Machhada, A. *et al.* Optogenetic Stimulation of Vagal Efferent Activity Preserves Left Ventricular Function in Experimental Heart Failure. *JACC: Basic to Translational Science* **5**, 799–810 (2020).

62. Mastitskaya, S. *et al.* Cardioprotection evoked by remote ischaemic preconditioning is critically dependent on the activity of vagal pre-ganglionic neurones. *Cardiovascular Research* **95**, 487–494 (2012).

63. Heldmaier, G., Braulke, L., Flick, J. & Ruf, T. Multiple ultradian rhythms of metabolism, body temperature and activity in Djungarian hamsters. *J Comp Physiol B* **194**, 501–518 (2024).

64. Fishbein, M. C. *et al.* Early phase acute myocardial infarct size quantification: validation of the triphenyl tetrazolium chloride tissue enzyme staining technique. *Am Heart J* **101**, 593–600 (1981).